pubs.acs.org/Biomac

Article

Multifunctional Dendrimer-Entrapped Gold Nanoparticles for Labeling and Tracking T Cells Via Dual-Modal Computed Tomography and Fluorescence Imaging

Meixiu Chen, Oshra Betzer, Yu Fan, Yue Gao, Mingwu Shen, Tamar Sadan, Rachela Popovtzer,* and Xiangyang Shi*

Cite This: *Biomacromolecules* 2020, 21, 1587−1595

Read Online

ACCESS | Metrics & More | Article Recommendations | Supporting Information

ABSTRACT: Nanosystems for monitoring and tracking T cells provide an important basis for evaluating the functionality and efficacy of T cell-based immunotherapy. To this end, we designed herein an efficient nanoprobe for T cell monitoring and tracking using poly(amidoamine) (PAMAM) dendrimer-entrapped gold nanoparticles (Au DENPs) conjugated with Fluo-4 for dual-mode computed tomography (CT) and fluorescence imaging. In this study, PAMAM dendrimers of generation 5 (G5) were modified with hydroxyl-terminated polyethylene glycol (PEG) and then used to entrap 2.0 nm Au NPs followed by acetylation of the excess amine groups on the dendrimer surface. Subsequently, the calcium ion probe was covalently attached to the dendrimer nanohybrids through the PEG hydroxyl end groups to gain the functional $\{(Au^0)_{25}$-G5.NHAc-$(PEG)_{14}$-$(Fluo\text{-}4)_2\}$ nanoprobe. This nanoprobe had excellent water solubility, high X-ray attenuation coefficient, and good cytocompatibility in the given concentration range, as well as a high T cell labeling efficiency. Confocal microscopy and flow cytometry results demonstrated that the nanoprobe was able to fluorescently sense activated T cells. Moreover, the nanoprobe was able to realize both CT and fluorescence imaging of subcutaneously injected T cells in vivo. Thus, the developed novel dendrimer-based nanosystem may hold great promise for advancing and improving the clinical application of T cell-based immunotherapy.

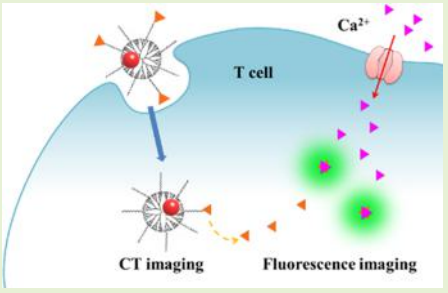

INTRODUCTION

Over the last decade, cancer therapy has evolved from nonspecific cytotoxic therapies to more selective and mechanism-based therapeutics. Unlike traditional cancer treatments, such as chemotherapy and radiotherapy, which are external treatments with many side effects on healthy tissues, cancer immunotherapy harnesses the power and specificity of the body's own immune system for treatments.[1−3] This approach also has the potential to prevent metastatic growth, which cannot be eliminated using traditional local treatments.[4] Among various types of immunotherapeutic treatments,[3,5−10] adoptive cell transfer therapy (ACT) using modified or enhanced T cells has recently gained increasing attention due to its ability to boost the natural ability of immune cells to fight cancer.[11] Various effector T cells have been explored for ACT, including tumor-infiltrating lymphocytes, T cell receptor (TCR)-engineered T cells,[7] and chimeric antigen receptor (CAR) T cells.[12,13] Following administration of such cells and antigen recognition by the TCR or CAR, activation and proliferation of the T cells can be achieved, ultimately leading to cancer cell killing via cytotoxin release.[14]

In vivo monitoring of the activity, migration, and biodistribution patterns of T cells for immunotherapy remains an open challenge. Addressing this challenge is crucial for answering basic questions regarding the cells' action mechanism and for facilitating clinical translation, particularly for treatment of solid tumors. Development of efficient cell monitoring and tracking techniques can greatly advance T cell-based immunotherapy.[15]

Nanomaterials, such as mesoporous silica,[16−18] nanogels,[19] nanocrystals,[20] and dendrimers,[21,22] can serve as carriers for various imaging agents,[23,24] thus forming nanoscale systems for multimodal imaging.[25−28] Among these nanomaterials, poly(amidoamine) (PAMAM) dendrimers are emerging as outstanding carriers due to their versatile branched architecture and flexibility of modification owing to the large number of surface-modifiable functional groups.[26−29] Previously, we developed a fifth-generation (G5) PAMAM dendrimer/carbon dot hybrid that can monitor cancer cells through fluorescence imaging due to the existence of carbon dots.[29] We have also shown that dendrimer-entrapped gold nanoparticles (Au DENPs) enable computed tomography (CT) imaging of

Received: January 31, 2020
Revised: March 6, 2020
Published: March 10, 2020

https://dx.doi.org/10.1021/acs.biomac.0c00147
Biomacromolecules 2020, 21, 1587−1595

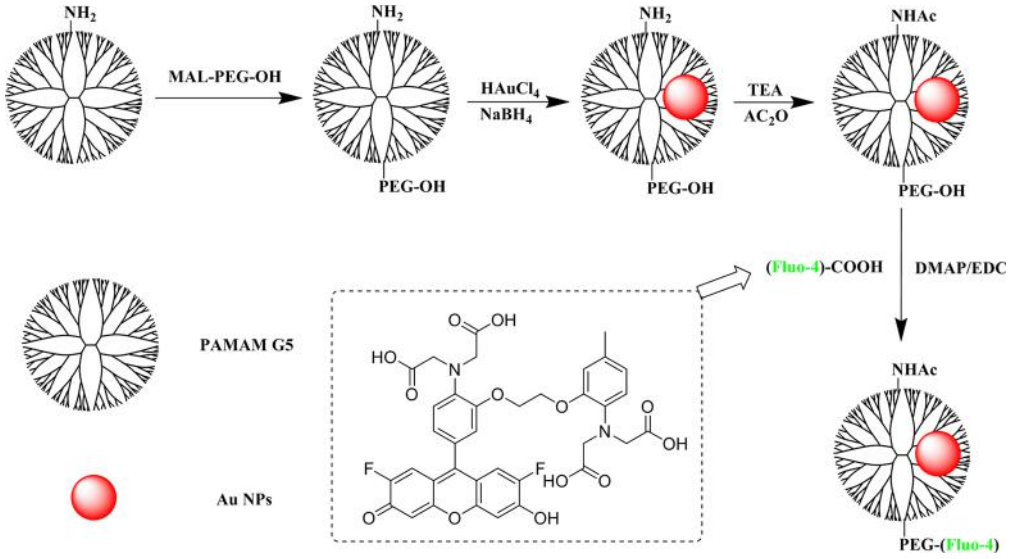

Figure 1. Schematic illustration of the synthesis of $\{(Au^0)_{25}$-G5.NHAc-$(PEG)_{14}$-$(Fluo\text{-}4)_2\}$ DENPs. TEA, Ac_2O, DMAP, and EDC represent triethylamine, acetic anhydride, 4-dimethylaminopyridine, and 1-ethyl-3-(3-dimethylaminopropyl) carbodiimide hydrochloride, respectively.

specific tissue in vivo[30−32] and that Au NPs can be employed for in vivo tracking of therapeutic cells and exosomes through CT imaging.[15,33−36]

In unstimulated T cells, the concentration of free calcium ions (Ca^{2+}) remains at a low level and considerably rises following binding of the T cell receptor to an antigen. The increase of cellular Ca^{2+} plays a central role in coordinating downstream T cell responses, including cell proliferation and induction of cancer cell killing.[17,18,37−39] Therefore, calcium signals can serve as a directly detectable parameter of T cell activation, indicating translation into functional responses. Recent development of various reliable and easy-to-use indicators of intracellular Ca^{2+} has significantly advanced this field of research. Among these indicators, Fluo-4 is an excellent candidate for cytoplasmic Ca^{2+} signal probing due to its high calcium affinity, ease of loading into cells, and bright fluorescence emission.[40] For instance, Li et al.[41] has conjugated Fluo-4 to upconversion NPs and used them to detect cytosol Ca^{2+} in HeLa cell lines and liver tissues after $CaCl_2$ injection. However, to promote T cell-based immunotherapy, it is essential to examine the utility of calcium-based nanoprobes for live sensing of T cell activation. In addition, a dual-modal imaging nanoprobe, combining two types of imaging agents, has the potential to provide enhanced and comprehensive functional information in vivo.[42]

Previously, we have shown that dendrimers can be used as a versatile platform to load dual types of imaging agents for SPECT/CT,[43,44] MR/CT,[45,46] or SPECT/MR[47] imaging of tumors. The major advantages to use dendrimers as a platform rely on their unique structural features that allow one to entrap inorganic NPs as one type of imaging agent within their interiors and surface modify the other one type or two types of imaging agents on their periphery to achieve dual-mode imaging.[48] With the prior achievements related to the dendrimer-based imaging platform, it is reasonable to hypothesize that a dual-modal imaging nanoprobe combining CT with fluorescence imaging may be developed for tracking T cells in vitro and in vivo.

In this present work, we designed a nanoprobe using multifunctional dendrimers as a platform to incorporate Au NPs for CT imaging and Fluo-4 for calcium-ion sensing to probe the location and activity of T cells. G5 PAMAM dendrimers were linked to PEG with a hydroxyl end group, entrapped with Au NPs inside their internal cavities, acetylated to neutralize the leftover amine terminal groups, and finally covalently conjugated with Fluo-4 (Figure 1). The generated Au DENP-based nanoprobe was systematically characterized using different techniques. Cytotoxicity and cellular uptake assays were carried out to examine the cytocompatibility of the probe to T cells and the probe's ability to be endocytosed by T cells for probing the activity of them via Ca^{2+}-mediated fluorescence sensing. Lastly, activated T cells preloaded with the probe were subcutaneously injected to mice and were then tracked via CT/fluorescence imaging. To our knowledge, this is the very first example to develop a dendrimer-based nanoprobe to track the location and activity of T cells via dual-mode CT/fluorescence imaging, which is important for live in vivo tracking of the fate and functionality of T cells in immunotherapy.

EXPERIMENTAL SECTION

Synthesis of $\{(Au^0)_{25}$-G5.NHAc-$(PEG)_{14}$-$(Fluo\text{-}4)_2\}$ DENPs. G5.NH_2-(PEG-OH) and $\{(Au^0)_{25}$-G5.NH_2-(PEG-OH)$\}$ DENPs were synthesized according to protocols reported in the literature.[31,49] Briefly, Mal-PEG-OH (18.5 mg, in 5 mL of H_2O) was added to the G5.NH_2 solution (10.0 mg, in 3 mL of H_2O) under stirring at room temperature for 24 h. The mixture was dialyzed against water for 3 days using a dialysis membrane having a molecular weight cutoff (MWCO) of 8000−14,000 and freeze-dried to obtain the product of G5.NH_2-(PEG-OH) dendrimers.

Next, $HAuCl_4$ solution (66.3 μL, 30 mg/mL) was dropwise added to the solution of the above G5.NH_2-(PEG-OH) dendrimers dissolved in 10 mL of water under magnetic stirring for 30 min followed by a quick addition of $NaBH_4$ solution (92.0 μL, 10 mg/mL in water). The mixture solution was then stirred for 3 h, dialyzed against water for 3 days using the same membranes described above, and freeze-dried to obtain the product of $\{(Au^0)_{25}$-G5.NH_2-(PEG-OH)$\}$ DENPs. Next, the $\{(Au^0)_{25}$-G5.NH_2-(PEG-OH)$\}$ DENPs (21.3 mg) were dissolved in 5 mL of water in which 25 μL of triethylamine (density 1.08 g/mL) was added while stirring for 30 min. This was followed by addition of 31.8 μL of acetic anhydride (density 0.726 g/mL) to neutralize the remaining dendrimer surface

https://dx.doi.org/10.1021/acs.biomac.0c00147
Biomacromolecules 2020, 21, 1587−1595

amines under stirring overnight. The reaction mixture was dialyzed against water for 3 days and lyophilized to obtain the $\{(Au^0)_{25}$-G5.NHAc-(PEG-OH)$\}$ DENPs.

Finally, under dark conditions, 1-ethyl-3-(3-dimethylaminopropyl) carbodiimide hydrochloride (1 mg/mL, in 1.3 mL of DMSO) was added to Fluo-4 pentasodium salt solution (1.0 mg, in 1 mL of DMSO) under stirring for 30 min. Then the activated Fluo-4 was mixed with the solution of $\{(Au^0)_{25}$-G5.NHAc-(PEG-OH)$\}$ DENPs (20.5 mg, in 5 mL of DMSO) under stirring for 30 min. After that, a 4-dimethylaminopyridine (DMAP) solution (0.41 mg/mL, in 100 μL of DMSO) was dropwise added to the above mixture under stirring for additional 3 days. Finally, the product of $\{(Au^0)$ -G5.NHAc-(PEG)-(Fluo-4)$\}$ DENPs was obtained by dialysis (MWCO = 8000−14,000 Da) and lyophilization steps described above.

T Cell Extraction, Identification, and Culture. All animal experiments were carried out after approval by the ethical committee for animal care of Donghua University and according to the policy of the National Ministry of Health. C57BL/6 mice were purchased from Shanghai Laboratory Animal Center (SLAC, Shanghai, China). T cells were extracted from the C57BL/6 mice through a nylon hair column according to the literature.[50,51] The extracted T cells were centrifuged to remove the supernatant, resuspended in 2 mL of phosphate-buffered saline (PBS), and stained with CD3 monoclonal antibody (17A2, fluorescein isothiocyanate (FITC)-labeled, 5−10 μL) and rat IgG2b kappa isotype control (eB149/10H5, FITC-labeled, 5−10 μL). After mixing thoroughly, the cells were placed at 0 °C in the dark for 15 min, washed with PBS to remove excess dyes, and resuspended in 300 μL of PBS before flow cytometry analysis (BD FACS Calibur flow cytometer, Franklin Lake, NJ) where the percentage of CD3+ T cells indicates the purity of T cells. The extracted T cells were cultured in an RPMI 1640 medium supplemented with 10% FBS and 1% penicillin−streptomycin. The cells were incubated at 37 °C in a Thermo Scientific cell incubator (Waltham, MA) with 5% CO_2.

T Cell Activation. T cells were activated by phorbol 12-myristate 13-acetate (PMA) and ionomycin (Iono) according to well-established protocols.[52,53] The concentrations of PMA and Iono were set at 100 ng/mL and 1 μg/mL, respectively.

Detection of Cytokines in T Cells. The cytokines Interferon-γ (IFN-γ) and Interleukin-2 (IL-2) were chosen as indicators for T cell activation by PMA/Iono. To detect these cytokines, T cells were cultured in 48-well plates at a density of 1×10^5 cells per well with 200 μL of fresh RPMI 1640 medium. At different time points (0, 6, 12, 18, and 24 h), the medium was replaced with a fresh RPMI 1640 medium containing 100 ng/mL PMA and 1 μg/mL Iono, and then the plate was centrifuged to collect the supernatants. The standard solution, enzyme working solution, chromogenic substrates, and termination solution were prepared in advance. Cytokines were detected according to the steps described in the instructions for both the Mouse IFN-γ enzyme-linked immunosorbent assay (ELISA) Kit and Mouse IL-2 ELISA Kit, respectively, and each sample was measured using three parallel wells of cells. The absorbance of each well was measured at 450 nm using a Thermo Scientific Multiskan MK3 ELISA reader (Thermo Scientific, Waltham, MA) within 10 min after the termination solution was added.

Probing T Cell Activity. T cells were cultured in a 48-well plate with a density of 2×10^5 cells per well overnight under normal cell culture conditions (5% CO_2, 37 °C). After stimulated by PMA/Iono for 0, 4, or 18 h, T cells were incubated with the $\{(Au^0)_{25}$-G5.NHAc-$(PEG)_{14}$-$(Fluo\text{-}4)_2\}$ DENPs (2.5 μM) for 4 h. Then the treated T cells were collected and washed three times with PBS. The cells were imaged by a Zeiss confocal laser scanning microscope (Jena, Germany). For quantitative analysis, the relative fluorescence intensity of the cells was measured by flow cytometry. T cells treated with PBS were used as control. For further comparison, after stimulated by PMA/Iono for 0, 4, or 18 h, T cells were incubated with the Fluo-4, AM probe (6 μM) for 4 h and then qualitatively and quantitatively analyzed under the same conditions.

Subcutaneous CT/Fluorescence Imaging of T Cells In Vivo. T cells were incubated with an RPMI 1640 medium containing $\{(Au^0)_{25}$-G5.NHAc-$(PEG)_{14}$-$(Fluo\text{-}4)_2\}$ DENPs (2.5 μM) for 4 h and then collected in 1.5-mL Eppendorf tubes. Each nude mouse was injected subcutaneously with 5×10^6 T cells suspended in 100 μL of saline and scanned by a dual-source SOMATOM Definition Flash CT system (Siemens, Erlangen, Germany) using parameters described in Supporting Information at 5 min post-injection. For fluorescence imaging of T cells in vivo, the T cells were first activated by PMA/Iono for 18 h and cocultured with the $\{(Au^0)_{25}$-G5.NHAc-$(PEG)_{14}$-$(Fluo\text{-}4)_2\}$ DENPs (2.5 μM) at the last 4 h of activation. Activated T cells (5×10^6 cells in 100 μL of saline) loaded with the $\{(Au^0)_{25}$-G5.NHAc-$(PEG)_{14}$-$(Fluo\text{-}4)_2\}$ DENPs were harvested and subcutaneously injected into the back of each nude mouse. The mice were fluorescence-imaged using a real-time ultrahigh-resolution imaging and analysis system VISQUE Invivo Smart (Vieworks Co., Ltd., Gyeonggi-do, Korea). The whole-body fluorescence distribution patterns were acquired at 5 min post-injection. See more experimental details in Supporting Information.

RESULTS AND DISCUSSION

Synthesis and Characterization of $\{(Au^0)_{25}$-G5.NHAc-$(PEG)_{14}$-$(Fluo\text{-}4)_2\}$ DENPs. Due to the versatility of dendrimer nanotechnology that allows for the interior entrapment of NPs and the periphery surface functionalization, we designed multifunctional Au DENPs as a nanoprobe. Amine-surfaced G5 PAMAM dendrimers were partially modified with Mal-PEG-OH, entrapped with Au NPs inside their internal cavities, acetylated to neutralize their remaining amine groups on the dendrimer surface, and finally covalently linked with a calcium-ion probe Fluo-4 by esterification of the carboxyl group of Fluo-4 with the hydroxyl group on the PEG to form the nanoprobe of $\{(Au^0)_{25}$-G5.NHAc-$(PEG)_{14}$-$(Fluo\text{-}4)_2\}$ DENPs (Figure 1).

The intermediate products synthesized in each step such as G5.NH_2-PEG-OH, $\{(Au^0)_{25}$-G5.NHAc-$(PEG\text{-}OH)_{14}\}$, and the final product of $\{(Au^0)_{25}$-G5.NHAc-$(PEG)_{14}$-$(Fluo\text{-}4)_2\}$ were characterized by ^{1}H NMR (Figure S1). The specific peak at 3.7 ppm can be assigned to the methylene proton peak of PEG, indicating the successful linking of Mal-PEG-OH on the surface of G5.NH_2 dendrimers (Figure S1a). Figure S1b shows a single peak at 1.88 ppm that can be ascribed to the $-COCH_3$ protons, validating the success of the dendrimer remaining terminal amine acetylation. Figure S1c shows the proton peaks of aromatic rings around 6−8 ppm, suggesting that the probe Fluo-4 has been covalently bound to the surface of the dendrimers. Through NMR peak integration, we can calculate that 13.6 PEG molecules, 68 acetyl groups, and 2.4 Fluo-4 acid have been linked to each G5 PAMAM dendrimer.

We further measured the surface potentials and hydrodynamic sizes of dendrimers and derivatives at different synthesis stages (Table S1). The surface potentials of G5.NH_2-$(PEG\text{-}OH)_{14}$ and $\{(Au^0)_{25}$-G5.NH_2-$(PEG\text{-}OH)_{14}\}$ seem to have no appreciable changes (from 34.7 to 40.3 mV) before and after Au NP entrapment. However, after acetylation and further conjugation with Fluo-4, the surface potentials of both $\{(Au^0)_{25}$-G5.NHAc-$(PEG\text{-}OH)_{14}\}$ and $\{(Au^0)_{25}$-G5.NHAc-$(PEG)_{14}$-$(Fluo\text{-}4)_2\}$ remain to be close to neutral, suggesting the success of the acetylation of dendrimer leftover terminal amines. The hydrodynamic sizes of all dendrimer derivatives before Fluo-4 conjugation are all around 203.1−207.1 nm, while after conjugation with Fluo-4, the Au DENPs have decreased hydrodynamic size. This suggests that their aggregation state changes to be more dispersed after last-step Fluo-4 conjugation.

https://dx.doi.org/10.1021/acs.biomac.0c00147
Biomacromolecules 2020, 21, 1587−1595

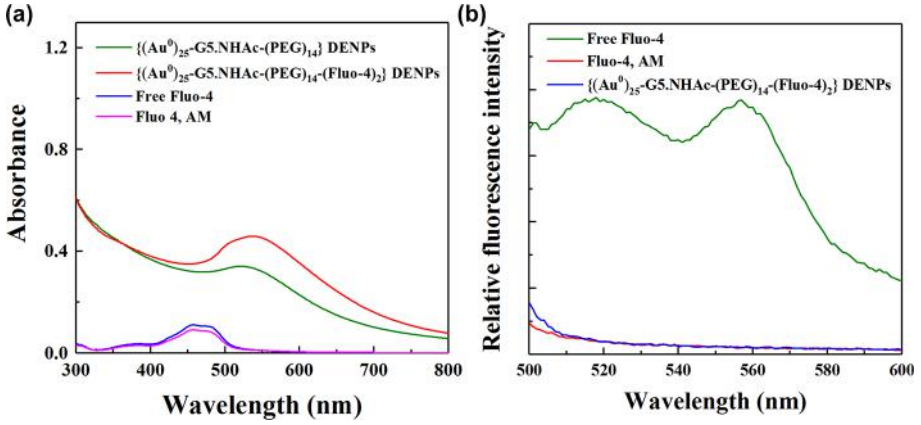

Figure 2. (a) UV−vis spectra of free Fluo-4, Fluo-4, AM, and the intermediate and final DENPs $\{(Au^0)_{25}$-G5.NHAc-(PEG-OH)$_{14}\}$ and $\{(Au^0)_{25}$-G5.NHAc-(PEG)$_{14}$-(Fluo-4)$_2\}$. (b) Fluorescence emission spectra of free Fluo-4, Fluo-4, AM, and $\{(Au^0)_{25}$-G5.NHAc-(PEG)$_{14}$-(Fluo-4)$_2\}$ DENPs dissolved or dispersed in Ca-EGTA buffer ([Ca] = 39 μM) at 488 nm excitation wavelength.

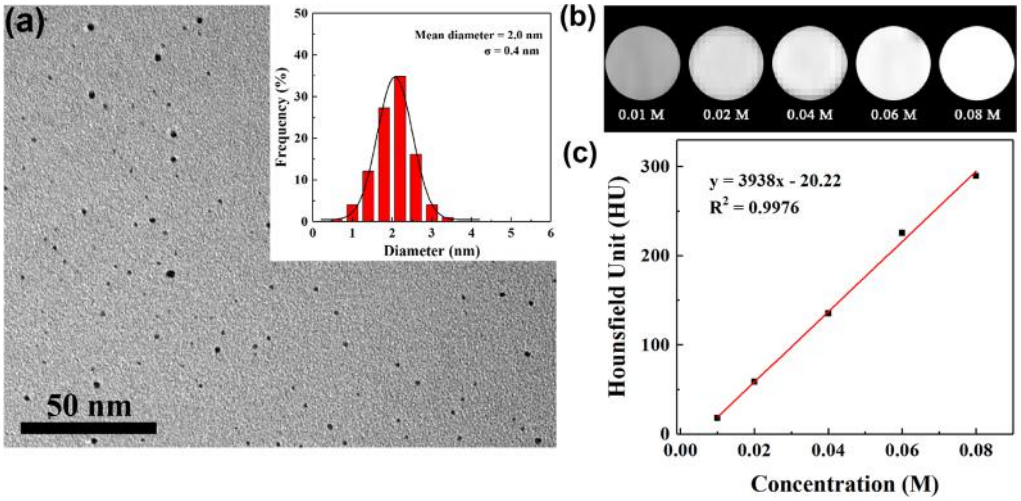

Figure 3. (a) TEM image and Au core size distribution histogram of the $\{(Au^0)_{25}$-G5.NHAc-(PEG)$_{14}$-(Fluo-4)$_2\}$ DENPs. (b) CT images and (c) CT values of $\{(Au^0)_{25}$-G5.NHAc-(PEG)$_{14}$-(Fluo-4)$_2\}$ DENPs at different Au concentrations.

Further, the entrapment of the Au NPs within the dendrimers was validated by UV−vis spectrometry, where a surface plasmon resonance peak of Au NPs around 520 nm emerges (Figure 2a). Quantitative measurement of gold content by inductively coupled plasma-optical emission spectroscopy (ICP-OES) reveals that there are 25 gold atoms entrapped within each G5 PAMAM dendrimer, corresponding to the initial Au salt/dendrimer molar ratio. This means that the added Au salt within the dendrimer solution can be completely reduced to form zero-valent Au. It should be noted that we selected the Au salt/dendrimer molar ratio at 25:1 instead of a larger ratio that could be beneficial for more sensitive CT imaging. This is because Au DENPs formed with a Au salt/dendrimer molar ratio of 25:1 display the optimized gene delivery efficiency,[54] and our future work will be focused on the use of the developed probe for gene delivery. Figure 2a also shows that the absorbance of $\{(Au^0)_{25}$-G5.NHAc-(PEG)$_{14}$-(Fluo-4)$_2\}$ DENPs around 400−520 nm is higher than those of free Fluo-4, commercial Fluo-4 acetoxymethyl ester derivative (Fluo-4, AM), and Fluo-4-free $\{(Au^0)_{25}$-G5.NHAc-(PEG-OH)$_{14}\}$ DENPs at the same concentration, demonstrating that Fluo-4 has been successfully linked to the dendrimers.

Fluorescence intensities of free Fluo-4, Fluo-4, AM, and $\{(Au^0)_{25}$-G5.NHAc-(PEG)$_{14}$-(Fluo-4)$_2\}$ DENPs were examined in Ca-EGTA buffer solution ([Ca] = 39 μM). The fluorescence spectrum of free Fluo-4 after chelation with Ca^{2+} shows a peak at 520 nm, while Fluo-4, AM and $\{(Au^0)_{25}$-G5.NHAc-(PEG)$_{14}$-(Fluo-4)$_2\}$ DENPs do not show any apparent fluorescence signals under the same conditions (Figure 2b). In general, Fluo-4 without chelation of Ca^{2+} has no intrinsic fluorescence.[55] Fluo-4, AM and the $\{(Au^0)_{25}$-G5.NHAc-(PEG)$_{14}$-(Fluo-4)$_2\}$ DENPs both having a tight ester bond have no chances to chelate Ca^{2+} to produce fluorescence emission. This result, combined with ^{1}H NMR data, indicates that Fluo-4 has been stably conjugated to G5 PAMAM through ester bonds.

Next, the $\{(Au^0)_{25}$-G5.NHAc-(PEG)$_{14}$-(Fluo-4)$_2\}$ DENPs were observed using transmission electron microscopy (TEM) to analyze the morphology and size distribution of the entrapped Au core particles (Figure 3a). The Au cores are quite spherical with an average diameter of 2.0 nm. Further, the feasibility to use the Au DENPs as a CT contrast agent was assessed by CT phantom studies (Figure 3b,c). Apparently, the X-ray attenuation intensity of the Au DENPs increases with the increase of Au concentration and shows a linear relationship

https://dx.doi.org/10.1021/acs.biomac.0c00147
Biomacromolecules 2020, 21, 1587−1595

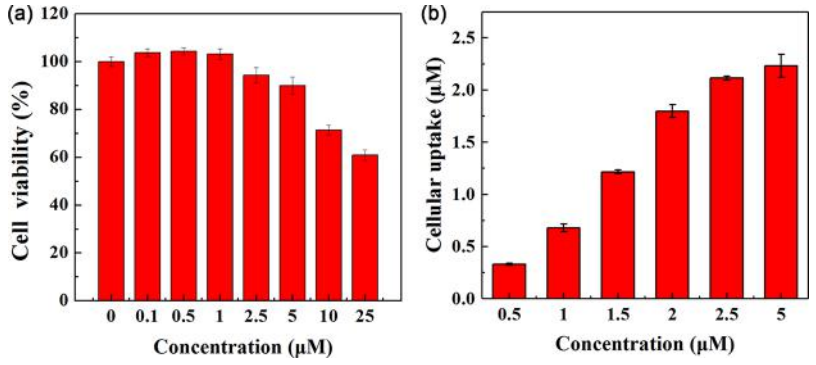

Figure 4. (a) CCK-8 assay of T cell viability after they were treated with the $\{(Au^0)_{25}$-G5.NHAc-$(PEG)_{14}$-$(Fluo\text{-}4)_2\}$ DENPs at different concentrations for 24 h. (b) Au uptake in T cells incubated with the $\{(Au^0)_{25}$-G5.NHAc-$(PEG)_{14}$-$(Fluo\text{-}4)_2\}$ DENPs at different concentrations for 4 h.

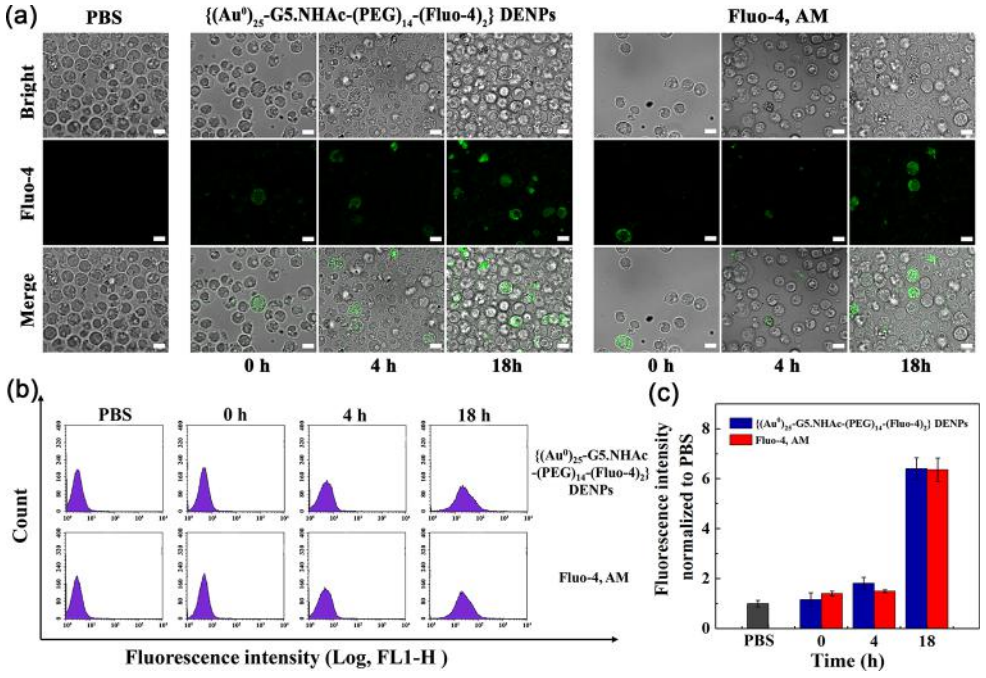

Figure 5. (a) Laser confocal microscopic images of T cells stimulated by PMA/Iono at different time points (0, 4, and 18 h, respectively) after T cells were incubated with the $\{(Au^0)_{25}$-G5.NHAc-$(PEG)_{14}$-$(Fluo\text{-}4)_2\}$ DENPs or Fluo-4, AM for 4 h (scale bar in each panel represents 5 μm). Panels (b) and (c) show the respective fluorescence histograms and relative fluorescence intensity of cells analyzed by flow cytometry.

versus the Au concentration (starting from 0.02 to 0.08 M). This means that the developed nanoprobe can be potentially used as a CT contrast agent, in agreement with our previous work.[56]

Cytotoxicity and T Cell Labeling Efficiency. T cells were extracted from C57BL/6 mice and checked to ensure their purity through the flow cytometry assay of the percentage of CD3+ T cells (Figure S2). Our data indicate the success of the extraction of T cells with reasonable batch-to-batch purity (73.8−93.5%). We first checked the cytotoxicity of the nanoprobe against T cells via the CCK-8 cell viability assay (Figure 4a). Clearly, the viability of T cells remains to be over 90% at a concentration of 5 μM. At a concentration of 10 μM or above, the cell viability starts to decrease. Therefore, we can safely conclude that, at the probe concentration up to 5 μM, the developed nanoprobe possesses good cytocompatibility.

Then the efficiency of T cell labeling with the nanoprobe of $\{(Au^0)_{25}$-G5.NHAc-$(PEG)_{14}$-$(Fluo\text{-}4)_2\}$ DENPs was measured by ICP-OES to quantify the Au uptake within the cells after incubation for 4 h. Through the Au quantification, the concentration of the uptaken nanoprobe was further calculated (Figure 4b). We show that the nanoprobe uptake by T cells gradually increases with the increase of nanoprobe concentration. At the highest concentration (5 μM), the cell uptake of the nanoprobe was determined to be 2.2 μM; hence, the loading efficiency of the probe within T cells was calculated to be 44%, which is lower than those at lower probe concentrations ranging from 66 to 89%. Based on the above results, we chose a probe concentration of 2.5 μM for subsequent experiments, as this concentration did not lead to the probe's toxicity to T cells, the probe labeling efficiency within the cells can reach as high as 84.6%, and the Fluo-4 concentration within the labeled cells is detectable.

Fluorescence Sensing of Activated T Cells. We next verified the ability of the nanoprobe to sense the activation state and functionality of T cells. In general, after T cell uptake of the nanoprobe, the ester bond between Fluo-4 and the nanoprobe can be cleaved by the intracellular esterase;[57]

https://dx.doi.org/10.1021/acs.biomac.0c00147
Biomacromolecules 2020, 21, 1587−1595

hence, the resulting free Fluo-4 can bind to the calcium ions within the cells to generate fluorescence emission. First, T cells were stimulated by phorbol myristate acetate (PMA)/ionomycin (Iono) according to the literature protocols.[52,53] The activation of T cells was verified through detection of cytokines of IFN-γ and IL-2 secreted by T cells (Figure S3). Clearly, after stimulation for 6 h, the IL-2 is the highest, while IFN-γ secretion is the highest at 18 h stimulation.

The activated T cells were incubated either with the nanoprobe or commercial Fluo-4, AM for 4 h before confocal microscopic observation and flow cytometric assay (Figure 5). Confocal micrographs of cells show that the fluorescence intensity of T cells gradually increases with the time of stimulation up to 18 h, indicating that the nanoprobe can detect an increased cell activation (Figure 5a), similar to the data obtained using the commercial Fluo-4, AM probe. Furthermore, flow cytometry assay data (Figure 5b,c) show the quantitative fluorescence intensity of T cells after stimulation for different time periods, confirming the effectiveness of the developed nanoprobe for fluorescence sensing of activated T cells. Our data also suggest that the covalently bound Fluo-4 on the dendrimer surface does not alter its fluorescence sensing ability of Ca^{2+} ions inside the T cells.

Dual-Mode CT/ Fluorescence Imaging of T Cells In Vivo. Next, we confirmed the feasibility to use the nanoprobe to monitor T cells in vivo via dual-mode CT/fluorescence imaging (Figure 6). T cells (5×10^6 cells, suspended in 100 μL of saline) loaded with the nanoprobe were subcutaneously injected into the back of each nude mouse, and CT scans were performed to evaluate T cell visibility. The probe-loaded T cells were clearly visible at 5 min post administration at the injection site with a high CT value of 37.05 HU (Figure 6a,b).

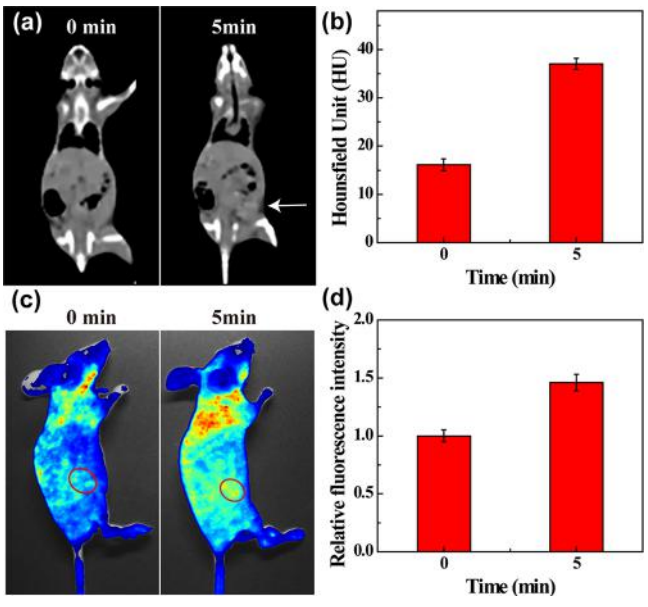

Figure 6. (a) In vivo CT images, (b) CT values, (c) fluorescence images, (d) and relative fluorescence intensity of T cells loaded with the $\{(Au^0)_{25}$-G5.NHAc-$(PEG)_{14}$-$(Fluo\text{-}4)_2\}$ DENPs after subcutaneous injection into the backs of mice before (0 min) and at 5 min post-injection of the T cells. For fluorescence imaging, the T cells were first activated by PMA/Iono for 18 h. The arrow and red circles indicate the injection sites.

This result indicates that the nanoprobe can be used to trace T cells in vivo via CT imaging.

We next checked the in vivo fluorescence imaging of activated T cells labeled with the nanoprobe. T cells were stimulated with PMA/Iono for 18 h, loaded with the nanoprobe for 4 h, and then subcutaneously injected into the back of each nude mouse followed by fluorescence imaging (Figure 6c,d). The relative fluorescence intensity of the injection site at 5 min post-injection increases significantly and shows a fluorescence intensity 1.5 times higher than the control mouse before injection. This result indicates that the nanoprobe can detect the site of activated T cells in vivo through fluorescence sensing. Taken together, our results give the first indication that the developed multifunctional dendrimer-based nanoprobe can trace and monitor T cells in vivo through dual-mode CT/fluorescence imaging and thus potentially enables live tracking of both the fate and functionality of T cells in vivo.

CONCLUSIONS

In summary, we developed a unique dendrimer-based multifunctional nanoprobe for labeling and tracking T cells via dual-modal CT/fluorescence imaging. The versatility of dendrimer nanotechnology enables the interior entrapment of Au NPs for CT imaging and periphery modification of the Fluo-4 dye for Ca^{2+}-mediated fluorescence sensing of the activity of T cells. The prepared nanoprobe is cytocompatible in the given concentration range, displays a high labeling efficiency of T cells (84.6%), and enables fluorescence sensing of activated T cells in vitro. With these properties owned along with its X-ray attenuation property, the designed dendrimer-based nanoprobe can be used for dual-mode CT/fluorescence imaging of T cells in vivo after subcutaneous injection. Overall, our study provides strong implications for the nanoprobe's potential to monitor and trace T cells in immunotherapy. In future work, we will investigate the nanoprobe's real-time T cell monitoring capabilities in a mouse tumor model. Such a system can afford an important basis to analyze T cell migration, biodistribution, and activation and to elucidate the underlying mechanisms and efficacy of T cell-based immunotherapy.

ASSOCIATED CONTENT

Supporting Information

The Supporting Information is available free of charge at https://pubs.acs.org/doi/10.1021/acs.biomac.0c00147.

More experimental details and additional data of surface potential and hydrodynamic size, NMR spectra, T cell purity analysis, and assay of cytokine secretion from T cells after stimulation (PDF)

AUTHOR INFORMATION

Corresponding Authors

Rachela Popovtzer – *Faculty of Engineering and the Institute of Nanotechnology & Advanced Materials, Bar-Ilan University, Ramat Gan 5290002, Israel*; Email: rachela.popovtzer@biu.ac.il

Xiangyang Shi – *State Key Laboratory for Modification of Chemical Fibers and Polymer Materials, International Joint Laboratory for Advanced Fiber and Low-dimension Materials, College of Chemistry, Chemical Engineering and Biotechnology,*

https://dx.doi.org/10.1021/acs.biomac.0c00147
Biomacromolecules 2020, 21, 1587–1595

Donghua University, Shanghai 201620, P. R. China; orcid.org/0000-0001-6785-6645; Email: xshi@dhu.edu.cn

Authors

Meixiu Chen − *State Key Laboratory for Modification of Chemical Fibers and Polymer Materials, International Joint Laboratory for Advanced Fiber and Low-dimension Materials, College of Chemistry, Chemical Engineering and Biotechnology, Donghua University, Shanghai 201620, P. R. China*

Oshra Betzer − *Faculty of Engineering and the Institute of Nanotechnology & Advanced Materials, Bar-Ilan University, Ramat Gan 5290002, Israel;* orcid.org/0000-0002-4429-7024

Yu Fan − *State Key Laboratory for Modification of Chemical Fibers and Polymer Materials, International Joint Laboratory for Advanced Fiber and Low-dimension Materials, College of Chemistry, Chemical Engineering and Biotechnology, Donghua University, Shanghai 201620, P. R. China*

Yue Gao − *State Key Laboratory for Modification of Chemical Fibers and Polymer Materials, International Joint Laboratory for Advanced Fiber and Low-dimension Materials, College of Chemistry, Chemical Engineering and Biotechnology, Donghua University, Shanghai 201620, P. R. China*

Mingwu Shen − *State Key Laboratory for Modification of Chemical Fibers and Polymer Materials, International Joint Laboratory for Advanced Fiber and Low-dimension Materials, College of Chemistry, Chemical Engineering and Biotechnology, Donghua University, Shanghai 201620, P. R. China;* orcid.org/0000-0002-1065-0854

Tamar Sadan − *Faculty of Engineering and the Institute of Nanotechnology & Advanced Materials, Bar-Ilan University, Ramat Gan 5290002, Israel*

Complete contact information is available at: https://pubs.acs.org/10.1021/acs.biomac.0c00147

Notes

The authors declare no competing financial interest.

■ ACKNOWLEDGMENTS

This study was financially supported by the National Key R&D Program (2017YFE0196200), the Science and Technology Commission of Shanghai Municipality (19XD1400100, 17540712000, and 18520750400), and the National Natural Science Foundation of China (81761148028 and 21773026). This work was also partially supported by the Israel Science Foundation Joint NSFC-ISF Research Grant (2533/17), the Ministry of Science and Technology Israel-China cooperation, and by the Council for Higher Education Postdoctoral Fellowship for Outstanding Woman in Science for O.B.

■ REFERENCES

(1) Esteva, F. J.; Hubbard-Lucey, V. M.; Tang, J.; Pusztai, L. Immunotherapy and Targeted Therapy Combinations in Metastatic Breast Cancer. *Lancet Oncol.* **2019**, *20*, e175−e186.

(2) DeSantis, C. E.; Lin, C. C.; Mariotto, A. B.; Siegel, R. L.; Stein, K. D.; Kramer, J. L.; Alteri, R.; Robbins, A. S.; Jemal, A. Cancer Treatment and Survivorship Statistics, 2014. *Ca-Cancer J. Clin.* **2014**, *64*, 252−271.

(3) Mellman, I.; Coukos, G.; Dranoff, G. Cancer Immunotherapy Comes of Age. *Nature* **2011**, *480*, 480−489.

(4) Coulie, P. G.; Van den Eynde, B. J.; van der Bruggen, P.; Boon, T. Tumour Antigens Recognized by T Lymphocytes: at the Core of Cancer Immunotherapy. *Nat. Rev. Cancer* **2014**, *14*, 135−146.

(5) Guo, Z.; Wang, X.; Cheng, D.; Xia, Z.; Luan, M.; Zhang, S. PD-1 Blockade and OX40 Triggering Synergistically Protects Against Tumor Growth in a Murine Model of Ovarian Cancer. *PLoS One* **2014**, *9*, e89350.

(6) Kunert, A.; Debets, R. Engineering T Cells for Adoptive Therapy: Outsmarting the Tumor. *Curr. Opin. Immunol.* **2018**, *51*, 133−139.

(7) Ye, B.; Stary, C. M.; Gao, Q.; Wang, Q.; Zeng, Z.; Jian, Z.; Gu, L.; Xiong, X. Genetically Modified T-Cell-Based Adoptive Immunotherapy in Hematological Malignancies. *J. Immunol. Res.* **2017**, *2017*, 5210459.

(8) Saint-Jean, M.; Knol, A.-C.; Volteau, C.; Quéreux, G.; Peuvrel, L.; Brocard, A.; Pandolfino, M.-C.; Saiagh, S.; Nguyen, J.-M.; Bedane, C.; Basset-Seguin, N.; Khammari, A.; Dréno, B. Adoptive Cell Therapy with Tumor-Infiltrating Lymphocytes in Advanced Melanoma Patients. *J. Immunol. Res.* **2018**, *2018*, 3530148.

(9) Kantoff, P. W.; Higano, C. S.; Shore, N. D.; Berger, E. R.; Small, E. J.; Penson, D. F.; Redfern, C. H.; Ferrari, A. C.; Dreicer, R.; Sims, R. B.; Xu, Y.; Frohlich, M. W.; Schellhammer, P. F.; IMPACT Study Investigators. Sipuleucel-T Immunotherapy for Castration-Resistant Prostate Cancer. *N. Engl. J. Med.* **2010**, *363*, 411−422.

(10) Pardoll, D. M. The Blockade of Immune Checkpoints in Cancer Immunotherapy. *Nat. Rev. Cancer* **2012**, *12*, 252−264.

(11) Roncarolo, M.-G.; Battaglia, M. Regulatory T-Cell Immunotherapy for Tolerance to Self Antigens and Alloantigens in Humans. *Nat. Rev. Immunol.* **2007**, *7*, 585−598.

(12) Miliotou, A. N.; Papadopoulou, L. C. CAR T-cell Therapy: A New Era in Cancer Immunotherapy. *Curr. Pharm. Biotechnol.* **2018**, *19*, 5−18.

(13) Salter, A. I.; Pont, M. J.; Riddell, S. R. Chimeric Antigen Receptor Modified T Cells: CD19 and the Road Beyond. *Blood* **2018**, *131*, 2621−2629.

(14) June, C. H.; O'Connor, R. S.; Kawalekar, O. U.; Ghassemi, S.; Milone, M. C. CAR T Cell Immunotherapy for Human Cancer. *Science* **2018**, *359*, 1361−1365.

(15) Meir, R.; Shamalov, K.; Betzer, O.; Motiei, M.; Horovitz-Fried, M.; Yehuda, R.; Popovtzer, A.; Popovtzer, R.; Cohen, C. J. Nanomedicine for Cancer Immunotherapy: Tracking Cancer-Specific T-Cells in Vivo with Gold Nanoparticles and CT Imaging. *ACS Nano* **2015**, *9*, 6363−6372.

(16) Xie, J.; Yong, Y.; Dong, X.; Du, J.; Guo, Z.; Gong, L.; Zhu, S.; Tian, G.; Yu, S.; Gu, Z.; Zhao, Y. Therapeutic Nanoparticles Based on Curcumin and Bamboo Charcoal Nanoparticles for Chemo-Photothermal Synergistic Treatment of Cancer and Radioprotection of Normal Cells. *ACS Appl. Mater. Interfaces* **2017**, *9*, 14281−14291.

(17) Xuan, M.; Shao, J.; Zhao, J.; Li, Q.; Dai, L.; Li, J. Magnetic Mesoporous Silica Nanoparticles Cloaked by Red Blood Cell Membranes: Applications in Cancer Therapy. *Angew. Chem., Int. Ed.* **2018**, *57*, 6049−6053.

(18) Yang, Y.; Li, J. Lipid, Protein and Poly (NIPAM) Coated Mesoporous Silica Nanoparticles for Biomedical Applications. *Adv. Colloid Interface Sci.* **2014**, *207*, 155−163.

(19) Sun, W.; Zhang, J.; Zhang, C.; Zhou, Y.; Zhu, J.; Peng, C.; Shen, M.; Shi, X. A Unique Nanogel-Based Platform for Enhanced Dual Mode Tumor MR/CT Imaging. *J. Mater. Chem. B* **2018**, *6*, 4835−4842.

(20) Yan, X.; Cui, Y.; Qi, W.; Su, Y.; Yang, Y.; He, Q.; Li, J. Self-Assembly of Peptide-Based Colloids Containing Lipophilic Nanocrystals. *Small* **2008**, *4*, 1687−1693.

(21) Khandare, J. J.; Jayant, S.; Singh, A.; Chandna, P.; Wang, Y.; Vorsa, N.; Minko, T. Dendrimer Versus Linear Conjugate: Influence of Polymeric Architecture on the Delivery and Anticancer Effect of Paclitaxel. *Bioconjugate Chem.* **2006**, *17*, 1464−1472.

(22) Tomalia, D. A.; Baker, H.; Dewald, J.; Hall, M.; Kallos, G.; Martin, S.; Roeck, J.; Ryder, J.; Smith, P. A New Class of Polymers: Starburst-Dendritic Macromolecules. *Polym. J.* **1985**, *17*, 117−132.

(23) Li, Z.; Zhang, Y.; Huang, L.; Yang, Y.; Zhao, Y.; El-Banna, G.; Han, G. Nanoscale "fluorescent stone": Luminescent Calcium

Fluoride Nanoparticles as Theranostic Platforms. *Theranostics* **2016**, *6*, 2380−2393.
(24) Lu, Y.; Li, L.; Lin, Z.; Li, M.; Hu, X.; Zhang, Y.; Peng, M.; Xia, H.; Han, G. Enhancing Osteosarcoma Killing and CT Imaging Using Ultrahigh Drug Loading and NIR-Responsive Bismuth Sulfide@ Mesoporous Silica Nanoparticles. *Adv. Healthcare Mater.* **2018**, *7*, 1800602.
(25) Zhou, B.; Xiong, Z.; Wang, P.; Peng, C.; Shen, M.; Mignani, S.; Majoral, J.-P.; Shi, X. Targeted Tumor Dual Mode CT/MR Imaging Using Multifunctional Polyethylenimine-Entrapped Gold Nanoparticles Loaded with Gadolinium. *Drug Delivery* **2018**, *25*, 178−186.
(26) Chen, Q.; Li, K.; Wen, S.; Liu, H.; Peng, C.; Cai, H.; Shen, M.; Zhang, G.; Shi, X. Targeted CT/MR Dual Mode Imaging of Tumors Using Multifunctional Dendrimer-Entrapped Gold Nanoparticles. *Biomaterials* **2013**, *34*, 5200−5209.
(27) Huang, K.; Li, Z.; Lin, J.; Han, G.; Huang, P. Two-Dimensional Transition Metal Carbides and Nitrides (MXenes) for Biomedical Applications. *Chem. Soc. Rev.* **2018**, *47*, 5109−5124.
(28) Lin, W.; Zhang, W.; Liu, S.; Li, Z.; Hu, X.; Xie, Z.; Duan, C.; Han, G. Engineering pH-Responsive BODIPY Nanoparticles for Tumor Selective Multimodal Imaging and Phototherapy. *ACS Appl. Mater. Interfaces* **2019**, *11*, 43928−43935.
(29) Li, D.; Fan, Y.; Shen, M.; Bányai, I.; Shi, X. Design of Dual Drug-Loaded Dendrimer/Carbon Dot Nanohybrids for Fluorescence Imaging and Enhanced Chemotherapy of Cancer Cells. *J. Mater. Chem. B* **2019**, *7*, 277−285.
(30) Zhou, B.; Zhao, L.; Shen, M.; Zhao, J.; Shi, X. A Multifunctional Polyethylenimine-Based Nanoplatform for Targeted Anticancer Drug Delivery to Tumors In Vivo. *J. Mater. Chem. B* **2017**, *5*, 1542−1550.
(31) Peng, C.; Zheng, L.; Chen, Q.; Shen, M.; Guo, R.; Wang, H.; Cao, X.; Zhang, G.; Shi, X. Pegylated Dendrimer-Entrapped Gold Nanoparticles for In Vivo Blood Pool and Tumor Imaging by Computed Tomography. *Biomaterials* **2012**, *33*, 1107−1119.
(32) Xiong, Z.; Wang, Y.; Zhu, J.; Li, X.; He, Y.; Qu, J.; Shen, M.; Xia, J.; Shi, X. Dendrimers Meet Zwitterions: Development of A Unique Antifouling Nanoplatform for Enhanced Blood Pool, Lymph Node and Tumor CT Imaging. *Nanoscale* **2017**, *9*, 12295−12301.
(33) Chemla, Y.; Betzer, O.; Markus, A.; Farah, N.; Motiei, M.; Popovtzer, R.; Mandel, Y. Gold Nanoparticles for Multimodal High-Resolution Imaging of Transplanted Cells for Retinal Replacement Therapy. *Nanomedicine* **2019**, *14*, 1857−1871.
(34) Guo, S.; Perets, N.; Betzer, O.; Ben-Shaul, S.; Sheinin, A.; Michaelevski, I.; Popovtzer, R.; Offen, D.; Levenberg, S. Intranasal Delivery of Mesenchymal Stem Cell Derived Exosomes Loaded with Phosphatase and Tensin Homolog siRNA Repairs Complete Spinal Cord Injury. *ACS Nano* **2019**, *13*, 10015−10028.
(35) Perets, N.; Betzer, O.; Shapira, R.; Brenstein, S.; Angel, A.; Sadan, T.; Ashery, U.; Popovtzer, R.; Offen, D. Golden Exosomes Selectively Target Brain Pathologies in Neurodegenerative and Neurodevelopmental Disorders. *Nano Lett.* **2019**, *19*, 3422−3431.
(36) Meir, R.; Betzer, O.; Motiei, M.; Kronfeld, N.; Brodie, C.; Popovtzer, R. Design Principles for Noninvasive, Longitudinal and Quantitative Cell Tracking with Nanoparticle-Based CT Imaging. *Nanomedicine* **2017**, *13*, 421−429.
(37) Christo, S. N.; Diener, K. R.; Hayball, J. D. The Functional Contribution of Calcium Ion Flux Heterogeneity in T Cells. *Immunol. Cell Biol.* **2015**, *93*, 694−704.
(38) Stathopulos, P. B.; Ikura, M. Structural Aspects of Calcium-Release Activated Calcium Channel Function. *Channels* **2014**, *7*, 344−353.
(39) Schwarz, E. C.; Qu, B.; Hoth, M. Calcium, Cancer and Killing: the Role of Calcium in Killing Cancer Cells by Cytotoxic T Lymphocytes and Natural Killer Cells. *Biochim. Biophys. Acta* **2013**, *1833*, 1603−1611.
(40) Gee, K. R.; Brown, K. A.; Chen, W.-N. U.; Bishop-Stewart, J.; Gray, D.; Johnson, I. Chemical and Physiological Characterization of Fluo-4 Ca^{2+}-Indicator Dyes. *Cell Calcium* **2000**, *27*, 97−106.
(41) Li, Z.; Lv, S.; Wang, Y.; Chen, S.; Liu, Z. Construction of LRET-Based Nanoprobe Using Upconversion Nanoparticles with Confined Emitters and Bared Surface as Luminophore. *J. Am. Chem. Soc.* **2015**, *137*, 3421−3427.
(42) Shi, Y.; Pan, Y.; Zhang, H.; Zhang, Z.; Li, M. J.; Yi, C.; Yang, M. A Dual-Mode Nanosensor Based on Carbon Quantum Dots and Gold Nanoparticles for Discriminative Detection of Glutathione in Human Plasma. *Biosens. Bioelectron.* **2014**, *56*, 39−45.
(43) Li, X.; Xiong, Z.; Xu, X.; Luo, Y.; Peng, C.; Shen, M.; Shi, X. ^{99m}Tc-Labeled Multifunctional Low-Generation Dendrimer-Entrapped Gold Nanoparticles for Targeted SPECT/CT Dual-Mode Imaging of Tumors. *ACS Appl. Mater. Interfaces* **2016**, *8*, 19883−19891.
(44) Xu, X.; Zhao, L.; Li, X.; Wang, P.; Zhao, J.; Shi, X.; Shen, M. Targeted Tumor SPECT/CT Dual Mode Imaging Using Multifunctional RGD-Modified Low Generation Dendrimer-Entrapped Gold Nanoparticles. *Biomater. Sci.* **2017**, *5*, 2393−2397.
(45) Xu, X.; Liu, K.; Wang, Y.; Zhang, C.; Shi, M.; Wang, P.; Shen, L.; Xia, J.; Ye, L.; Shi, X.; Shen, M. A Multifunctional Low-Generation Dendrimer-Based Nanoprobe for the Targeted Dual Mode MR/CT Imaging of Orthotopic Brain Gliomas. *J. Mater. Chem. B* **2019**, *7*, 3639−3643.
(46) Liu, J.; Xiong, Z.; Zhang, J.; Peng, C.; Klajnert-Maculewicz, B.; Shen, M.; Shi, X. Zwitterionic Gadolinium(III)-Complexed Dendrimer-Entrapped Gold Nanoparticles for Enhanced Computed Tomography/Magnetic Resonance Imaging of Lung Cancer Metastasis. *ACS Appl. Mater. Interfaces* **2019**, *11*, 15212−15221.
(47) Luo, Y.; Zhao, L.; Li, X.; Yang, J.; Guo, L.; Zhang, G.; Shen, M.; Zhao, J.; Shi, X. The Design of a Multifunctional Dendrimer-Based Nanoplatform for Targeted Dual Mode SPECT/MR Imaging of Tumors. *J. Mater. Chem. B* **2016**, *4*, 7220−7225.
(48) Qiao, Z.; Shi, X. Dendrimer-Based Molecular Imaging Contrast Agents. *Prog. Polym. Sci.* **2015**, *44*, 1−27.
(49) Zhu, J.; Zheng, L.; Wen, S.; Tang, Y.; Shen, M.; Zhang, G.; Shi, X. Targeted Cancer Theranostics Using Alpha-Tocopheryl Succinate-Conjugated Multifunctional Dendrimer-Entrapped Gold Nanoparticles. *Biomaterials* **2014**, *35*, 7635−7646.
(50) Li, S. Y.; Liu, Y.; Xu, C. F.; Shen, S.; Sun, R.; Du, X. J.; Xia, J. X.; Zhu, Y. H.; Wang, J. Restoring Anti-Tumor Functions of T cells via Nanoparticle-Mediated Immune Checkpoint Modulation. *J. Controlled Release* **2016**, *231*, 17−28.
(51) Hathcock, K. S. T Cell Enrichment by Nonadherence to Nylon. *Curr. Protoc. Immunol.* **1999**, *30*, 321−324.
(52) Rostaing, L.; Tkaczuk, J.; Durand, M.; Peres, C.; Durand, D.; de Préval, C.; Ohayon, F.; Abbal, M. Kinetics of Intracytoplasmic Th1 and Th2 Cytokine Production Assessed by Flow Cytometry Following In Vitro Activation of Peripheral Blood Mononuclear Cells. *Cytometry* **1999**, *35*, 318−328.
(53) Granzin, M.; Stojanovic, A.; Miller, M.; Childs, R.; Huppert, V.; Cerwenka, A. Highly Efficient IL-21 and Feeder Cell-Driven Ex Vivo Expansion of Human NK Cells with Therapeutic Activity in a Xenograft Mouse Model of Melanoma. *OncoImmunology* **2016**, *5*, e1219007.
(54) Shan, Y.; Luo, T.; Peng, C.; Sheng, R.; Cao, A.; Cao, X.; Shen, M.; Guo, R.; Tomás, H.; Shi, X. Gene Delivery Using Dendrimer-Entrapped Gold Nanoparticles as Nonviral Vectors. *Biomaterials* **2012**, *33*, 3025−3035.
(55) Beierlein, M.; Gee, K. R.; Martin, V. V.; Regehr, W. G. Presynaptic Calcium Measurements at Physiological Temperatures Using a New Class of Dextran-Conjugated Indicators. *J. Neurophysiol.* **2004**, *92*, 591−599.
(56) Fan, Y.; Tu, W.; Shen, M.; Chen, X.; Ning, Y.; Li, J.; Chen, T.; Wang, H.; Yin, F.; Liu, Y.; Shi, X. Targeted Tumor Hypoxia Dual-Mode CT/MR Imaging and Enhanced Radiation Therapy Using Dendrimer-Based Nanosensitizers. *Adv. Funct. Mater.* **2020**, DOI: 10.1002/adfm.201909285.
(57) Tsien, R. Y.; Pozzan, T.; Rink, T. J. Calcium Homeostasis in Intact Lymphocytes: Cytoplasmic Free Calcium Monitored with a

https://dx.doi.org/10.1021/acs.biomac.0c00147
Biomacromolecules 2020, 21, 1587−1595

New, Intracellularly Trapped Fluorescent Indicator. *J. Cell Biol.* **1982**, *94*, 325−334.

https://dx.doi.org/10.1021/acs.biomac.0c00147
Biomacromolecules 2020, 21, 1587−1595